CDF/ANAL/JET/GROUP/9486
Version 1.0
August 23, 2008

Study of Event Shapes in $p\bar{p}$ Collisions

L. Pinera[1], A. Korytov [2]

University of Florida

S. Jindariani[3]

Fermilab

Abstract

We present a study of event shape variables in $p\bar{p}$ collisions at $\sqrt{s} = 1.96$TeV. The observables studied are the transverse thrust and thrust minor, both defined over final state momenta perpendicular to the beam direction. The observables are measured using unclustered calorimeter energy. In addition to studies of the differential distributions, we present the evolution of event shape mean values as a function of the leading jet E_T. Data is compared to dedicated theoretical predictions (NLO+NLL) and subsequently to PYTHIA Monte Carlo with and without multiple parton interactions. In the presence of an underlying event the observables are found to significantly depart from the predictions of pure perturbative QCD. As a result, we construct an auxiliary quantity, a weighted difference of the mean values of the thrust and thrust minor, which is independent of the underlying event and study its evolution as a function of the leading jet energy.

[1]pinera@fnal.gov
[2]korytov@phys.ufl.edu
[3]sergo@fnal.gov

1 Introduction

This note, investigates the measurement of two event shape observables, the transverse thrust and thrust minor, which are proposed for study at hadron colliders.

Quite generally, event shapes describe geometric properties of the energy flow in QCD final states. In a sense, they are similar to jet-finding algorithms which can be used to categorize events according to their topology. However, they differ prominently in that event shapes encode information about the energy flow of an event in a continuous fashion; that is, a single parameter can describe, for example, the transition between a configuration with all particles flowing along a single axis and a configuration where the energy is distributed uniformly over solid angle. Event shapes therefore provide more detailed information about the final state geometry than a jet-finding algorithm which would necessarily classify every event as having some finite number of jets even when the energy is distributed isotropically. Furthermore, they have the advantage of being free of the arbitrariness associated with the jet definition (*i.e.*, being either cone or cluster in type, cone sizes, splitting/merging fractions, etc.).

Studies of QCD at hadron colliders have thus far focused on measurements such as the inclusive jet cross section as a function of jet transverse energy or the dijet cross section as a function of invariant mass. Both of these measurements feature steeply falling cross sections and suffer from large systematic uncertainties due to a limited knowledge of the jet energy scale. In contrast, the event shape variables studied are by definition normalized to the sum of the transverse energy in the event, which results in a cancelation of errors associated with an uncertainty in the absolute energy scale of the final state. Moreover, the differential distributions are normalized to the total cross section for selected events, thereby circumventing other uncertainties due to, for example, a measurement of the luminosity.

Event shapes have been studied extensively in e^+e^- and DIS experiments. In these environments they have provided a plethora of measurements of QCD parameters, particularly the strong coupling α_s and it's running [1]. In addition, their study has improved our understanding of the dynamics of soft pQCD [2], as well as a practical means of tuning Monte Carlo event generators [3]. Furthermore, theoretically they are sensitive to non-perturbative effects coming from hadronization. These non-perturbative corrections have been studied using phenomenological models of hadronization that are implemented in Monte Carlo event generators as well as power-law corrections to perturbative QCD predictions [4], [5].

By comparison, event shapes at hadron colliders have received far less attention, primarily due to the theoretical difficulties associated with the environment. From a theoretical point of view, a description over the full range of an event shape observable at a hadron collider requires not only perturbative QCD calculations (both fixed order and resummed results), but also the inclusion a phenomenological model of the underlying event. Only recently, have theorists been able to produce full perturbative QCD predictions at next-to-leading-order matched to next-to-leading-log (NLO+NLL) [6]. However, at present theorists have yet to incorporate even a simple model of beam

remnants. As result, the presence of the underlying event still casts some doubt as to whether these observables can be used to study the dynamics of perturbative QCD, much less hadronization corrections.

2 Definition of Observables

The event shapes studied here are defined as linear sums of the transverse momenta of particles in the final state. As such, they are infrared and colinear (IRC) safe which makes them calculable within perturbative QCD.

2.1 Transverse Thrust

The thrust is often considered the prototypical event shape observable. At a hadron collider it is defined as:

$$T_\perp \equiv \max_{\vec{n}_T} \frac{\sum_{i=0}^{n} |\vec{q}_{\perp i} \cdot \vec{n}_T|}{\sum_{i=0}^{n} |\vec{q}_{\perp i}|} \tag{1}$$

where the sum runs over all particles in the final state and the thrust axis, $\vec{n}_T$, is defined as the unit vector in the transverse plane which maximizes this expression. For a perfectly "pencil-like" event with only 2 outgoing particles, $T_\perp = 1$. In the case of a perfectly isotropic event the transverse thrust takes on the value $T_\perp = \frac{2}{\pi}$. Because the majority of event shapes vanish in the two-jet limit, it is convenient to define $\tau_\perp \equiv 1 - T_\perp$ which shares this property. Hereafter, any discussion of the observable called thrust shall refer to the quantity $\tau_\perp$.

2.2 Transverse Thrust Minor

Having defined the transverse thrust axis $\vec{n}_T$, one can define the transverse thrust minor:

$$T_{Min} \equiv \frac{\sum_{i=0}^{n} |\vec{q}_{\perp i} \cdot \vec{n}_m|}{\sum_{i=0}^{n} |\vec{q}_{\perp i}|}, \qquad \vec{n}_m = \vec{n}_T \times \hat{z} \tag{2}$$

The thrust axis $\vec{n}_T$ and the beam direction $\hat{z}$ together define the event plane in which the primary hard scattering occurs. Thus, the thrust minor can be viewed as a measure

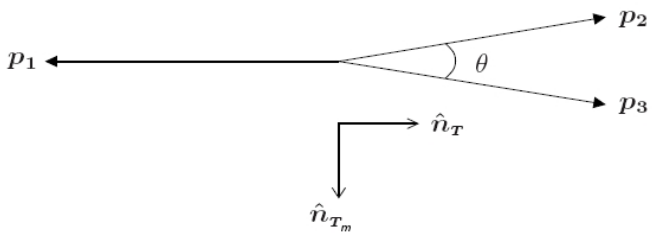

Figure 1: A three-jet event approaching the two-jet limit.

of the out-of-plane transverse momentum. Clearly, $T_{Min} = 0$ for a pencil-like event; when the momentum of both particles is directed entirely along the thrust axis. For an isotropic event the thrust minor assumes the value $\frac{2}{\pi}$.

When a three jet event approaches the two-jet limit, as shown in Fig. 1, it becomes clear that the observables have differing sensitivities to the opening angle θ:

$$\tau \sim 1 - \cos\theta \quad \sim \theta^2 \tag{3}$$

$$T_{Min} \sim \sin\theta \quad \sim \theta \tag{4}$$

Hence, it is expected that the thrust minor should be more sensitive to the effects of hadronization and particle decay than the thrust.

Theorists have proposed a number of other event shapes (broadenings, hemisphere masses, etc.) [6] whose definitions include some dependence on the longitudinal component of the final state particles' momenta. However, preliminary studies showed these observables to be sensitive to detector mismeasurement, particularly in the forward regions. As a result, we have chosen to focus on those observables defined exclusively in the transverse plane.

3 Dedicated Theoretical Predictions

The calculation of an event shape distribution in perturbative QCD is divided into two regimes: *fixed order* and *resummed* results. Almost all event shapes, including those considered here, have the property that large values of the observable coincide with the emission of one or more hard partons at large angles relative to the initial outgoing partons. In this regime, the differential cross section is well described by a traditional perturbative expansion in powers of the strong coupling. This method provides an accurate description for most of the range of the observable. However, as the event shape variable becomes small, this method breaks down. In fact, all fixed order calculations diverge in the limit that the observable goes to zero.

In this region, the differential cross section is primarily sensitive to gluon emission that is soft compared to the hard scale of the event and/or collinear to one of the hard

partons. Such radiation has relatively large emission probabilities due to logarithmic enhancements as well as the larger value of the coupling constant. In this case, each power of α_s in the perturbative expansion is accompanied by a coefficient that grows as $L \equiv \ln^2 \frac{1}{y}$ thus enhancing the importance of higher order terms in the series. The naive requirement that $\alpha_s \ll 1$ is no longer sufficient to render these terms negligible. This breakdown of the perturbative expansion arises because requiring the observable to be small essentially places a restriction on real emissions without a corresponding restriction on virtual contributions. The resulting incompleteness of the cancellations between logarithmically divergent real and virtual diagrams is the origin of the order by order enhancement in the perturbative expansion. To obtain a meaningful answer in the region $y \to 0$ it is necessary to perform an all-orders resummation of the enhanced terms.

At present, a technical restriction of any fully NLL resummations, is that the observable must be *global*, that is, it must be sensitive to emissions in all directions including arbitrarily close to the beam line. This requirement is in direct conflict with the experimental realities–namely the limited detector coverage in the forward region. However, the observables considered here are defined exclusively over the transverse plane. Therefore, for sufficiently large values of the maximum accessible pseudo-rapidity, the contribution from the excluded kinematic region is expected to give at most a small contribution to the observable [7] that would ultimately be significant only for very small values of the observable. For example, the full global predictions for the transverse thrust and thrust minor should remain valid for $\ln y \lesssim \eta_{max}$ where η_{max} is the maximum detector coverage.

It should be noted that theorists first proposed an alternative definition for event shapes at hadron colliders to specifically deal with the issue of limited detector coverage. As originally envisioned, the event shapes were to be defined over particles in some reduced central region and rendered "indirectly" global by the addition on an event by event basis of a "recoil" term. Such a term would be defined over particle momenta in the same central region as the rest of the observable but would introduce an indirect sensitivity to momenta outside that region. The proposed recoil term was essentially the vector sum of the transverse momenta in this central region (which by conservation of momentum is equal to the vector sum of transverse momenta outside the region). However, preliminary studies showed that there was almost no correlation between the event shapes (thrust and thrust minor) and the recoil term. As such, its effect was primarily to shift the mean and smear the distributions. As a result, this alternative definition was not pursued.

Finally, the dedicated theoretical predictions shown in this note (labeled "NLO+CAESAR" in figures) represent fixed order results at NLO accuracy matched to resummed results at NLL accuracy. Theorists' fixed order results are obtain from the MC integration program NLOJet++ [8] while their resummed results come by way of the "Computer Automated Expert Semi-Analytical Resummer" (CAESAR) []. A modified $\ln R$ matching scheme is adopted. These theoretical predictions include initial and final state radiation, but do not include any beam remnant models.

4 Pythia MC Samples

In order to understand the role of the underlying event and hadronization in shaping the distributions of the transverse thrust and thrust minor, we employ the Monte Carlo event generator PYTHIA to simulate multihadronic events in our detector. Our comparison to the dedicated theoretical predictions of Banfi, Salam, and Zanderighi proceeds in two stages. First, their results (NLO+CAESAR) are compared to PYTHIA 6.216 with all settings identical to the familiar PYTHIA Tune A except that multiple parton interactions (MPI) have been turned off. In this note, we refer to these samples simply as "PYTHIA". These generated events were placed through full detector simulation and are subject to the event selection criteria described in this text. We then compare theorists' predictions to the results of PYTHIA Tune A (which does include MPI) and subsequently to Data.

5 Treatment of the Underlying Event

At the time of this writing theorists have yet to include in their calculations of event shapes a model of the underlying event. As a result, a direct comparison of event shape distributions between data and the predictions of CAESAR is not possible. However, we believe that a quantity can be constructed from the average values of the observables that is independant of the UE. The evolution of this quantity with respect to the leading jet energy should then allow for meaningful comparison between theoretical predictions and measured data. To this end we begin by considering the definitions of the thrust (Eq. 1) and thrust minor (Eq. 2). Separating the final state into hard and soft components and recognizing that the thrust axis is determined almost entirely by the hard component, the transverse thrust and thrust minor can be written approximately as:

$$\tau_\perp \approx \frac{\sum q_\perp^{HARD} - \max_{\vec{n}_T} \sum q_\perp^{HARD} |\cos\phi^{HARD}|}{\sum |q_\perp^{HARD}| + \sum |q_\perp^{UE}|} + \frac{\sum q_\perp^{UE} |1 - \cos\phi^{UE}|}{\sum |q_\perp^{HARD}| + \sum |q_\perp^{UE}|} \tag{5}$$

$$T_{Min} = \frac{\sum q_\perp^{HARD} |\sin\phi^{HARD}|}{\sum |q_\perp^{HARD}| + \sum |q_\perp^{UE}|} + \frac{\sum q_\perp^{UE} |\sin\phi^{UE}|}{\sum |q_\perp^{HARD}| + \sum |q_\perp^{UE}|} \tag{6}$$

where ϕ^{HARD} and ϕ^{UE} represent the angle between the thrust axis and the hard and soft components respectively. The contribution of the underlying event is expected to be on average uniform over the transverse plane; therefore,

$$\langle |\cos\phi^{UE}| \rangle = \langle |\sin\phi^{UE}| \rangle = \frac{2}{\pi} \tag{7}$$

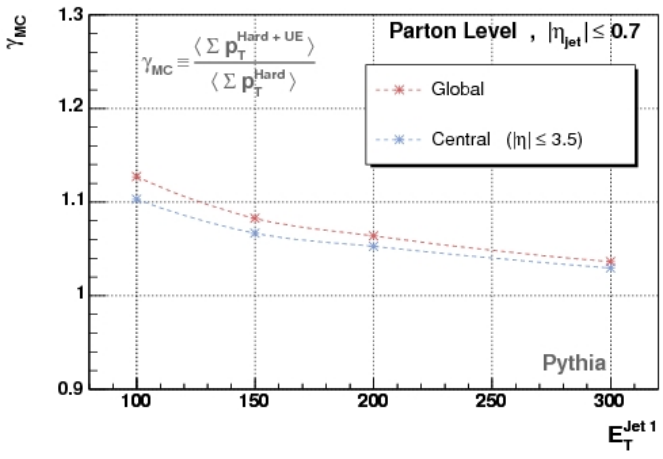

Figure 2: Ratio of the mean values of the $\sum p_T$ of particles between Pythia with and without multiple parton interactions as a function of the leading jet energy.

Taking a weighted difference between the mean values of the thrust and thrust minor we arrive at an expression whose numerator is independent of the underlying event.

$$\alpha \langle T_{Min} \rangle \; - \; \beta \langle \tau \rangle \approx$$
$$\alpha \left(\frac{\sum q_\perp^{HARD} |\sin \phi^{HARD}|}{\sum |q_\perp^{HARD}| + \sum |q_\perp^{UE}|} \right) - \beta \left(\frac{\sum q_\perp^{HARD} - \max_{\vec{n}_T} \sum q_\perp^{HARD} |\cos \phi^{HARD}|}{\sum |q_\perp^{HARD}| + \sum |q_\perp^{UE}|} \right) \quad (8)$$

Where $\alpha \equiv (1 - \frac{2}{\pi})$ and $\beta \equiv \frac{2}{\pi}$. The only trace of the underlying event in this expression is in the denominator, where its contribution is overshadowed by that of the hard scattering. Nevertheless, an additional factor, γ_{MC}, may be computed based on Monte Carlo generated with and without MPI to produce an expression entirely independent of the UE.

$$\gamma_{MC} \quad \equiv \quad \frac{\sum |q_\perp^{HARD}| + \sum |q_\perp^{UE}|}{\sum |q_\perp^{HARD}|} \quad (9)$$

then we can define a new quantity:

$$C(\langle \tau \rangle, \langle T_{Min} \rangle) \quad \equiv \quad \gamma_{MC} (\alpha \langle T_{Min} \rangle \; - \; \beta \langle \tau \rangle) \quad (10)$$

The factor γ_{MC} is plotted in Figure 2 as a function of the leading jet energy. Finally, it is the evolution of this quantity as a function of leading jet E_T that will allow for a meaningful comparison between Data and theorists' predictions.

Table 1: Summary of the data samples, trigger paths, and number of event present after selection criteria

E_T^1 (GeV)	Stntuple Set	Period	Events
100	Jet 50 (gjt2)	0d	$\sim$ 50 K
150	Jet 70 (gjt3)	0d	$\sim$ 18 K
200	Jet 100 (gjt4)	0d	$\sim$ 26 K
300	Jet 100 (gjt4)	0h+0i	$\sim$ 3 K

6 Data Samples and Event Selection

We report a measurement of event shapes in $p\bar{p}$ collisions at $\sqrt{s} = 1.96$ TeV. The results are presented for leading jet energies of 100, 150, 200, and 300 GeV. The data for the 100, 150, and 200 GeV samples were collected using single jet triggers with respective E_T thresholds of 50, 70, and 100 GeV during the period from February 2002 to August 2004. The events selected for the 300 GeV sample also come from the 100 GeV single jet trigger, but during a later data taking period corresponding to December 2004 to November 2006. Each of the trigger parths is unique and therefore each of the samples is statistically independent. This information is summarized in Table 1.

The following selections criteria is applied offline:

- Events are required to be on the Good Run List (v.19);
- Missing E_T significance cut is applied to remove events with large missing E_T. The cut values are 5.0, 6.0,7.0 $GeV^{1/2}$ for data collected using jet triggers with thresholds of 50,70,100 GeV respectively;
- Require events with 1 and only 1 primary reconstructed vertex of class 12;
- Z-position of the vertex is required to lie within $|Z_{vertex}| < 60$cm;
- Events are selected with at least 2 leading jets corrected to Level 7;
- The two leading jets are required to lie in the central region ($|\eta_{jet}^{1,2}| < 0.7$);
- Cut on the leading jet E_T with no additional cut on the second jet (motivated by theory.)

7 Measurement of Event Shapes

7.1 Calorimeter Towers

The measurement of event shapes is ultimately performed with unclustered calorimeter towers over the detector's full rapidity range ($|\eta| < 3.5$). Fig. 3 shows the η and ϕ distribution of towers in Data and MC. Clearly, an excess of towers is present in Data; however, the shapes of these distributions is well reproduced by the simulation. That is, the excess is uniformly distributed in $\eta - \phi$ space and was found not to be the result of "hot" towers. Restricting ourselves to the central region ($|\eta| < 1.1$) we observe that the excess appears over a wide range of transverse momentums, 100MeV$< p_T < 5$ GeV (see Fig. 4).

Plotting the distribution of towers as a function of the angle (ϕ_{nT}) between the 2D tower p_T and the transverse thrust axis n_T (Figure 5) we observe that the relative difference between data and MC is greatest in the region away from the primary energy flow (*i.e.*, away from of the transverse thrust axis, $\phi_{n_T} \sim \pi/2$). Finally we note that the average transverse energy density of towers in MC agrees quite well with data (Fig. 6). We return to the curious incident of the excess towers in the "away" region after a discussion of tracks in the central region.

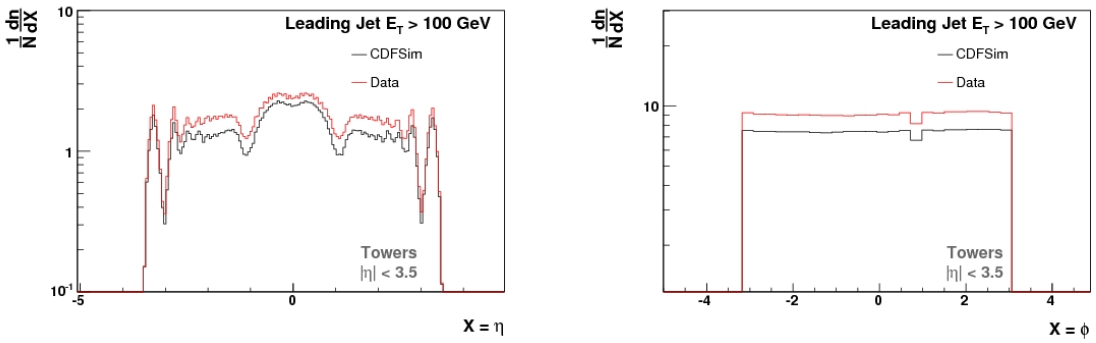

Figure 3: The distribution of calorimeter towers in η and ϕ over the full rapidity range of the detector. The distributions are normalized to the number of events in each sample. The label CDFSim refers to Pythia Tune A MC after full detector simulation.

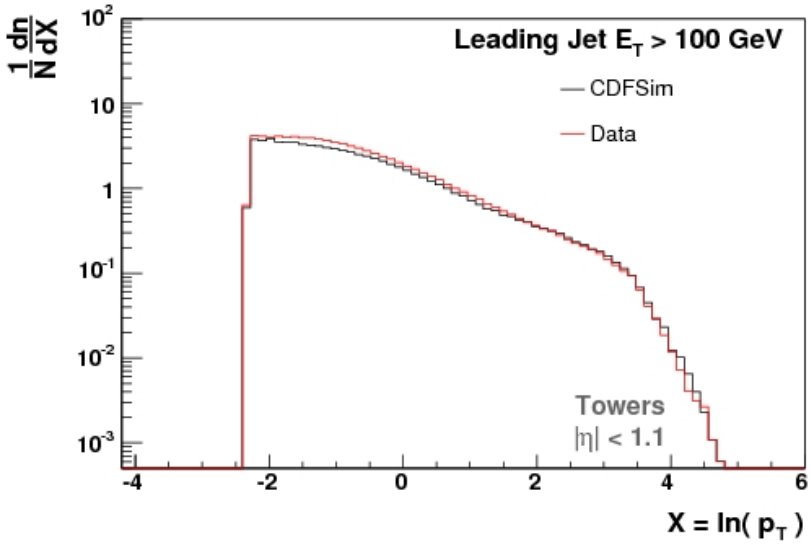

Figure 4: The transverse momentum distribution of calorimeter towers in the central region $|\eta| < 1.1$, normalized to the number of events in each sample. The label CDFSim refers to Pythia Tune A MC after full detector simulation.

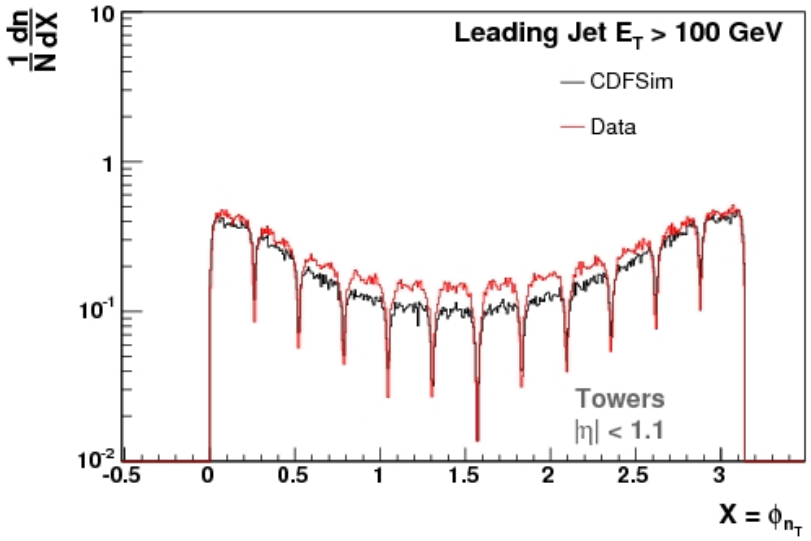

Figure 5: Distribution of towers over the central region $|\eta| < 1.1$ as a function of the angle between the 2D tower $\vec{p_T}$ and the transverse thrust axis $\vec{n_T}$

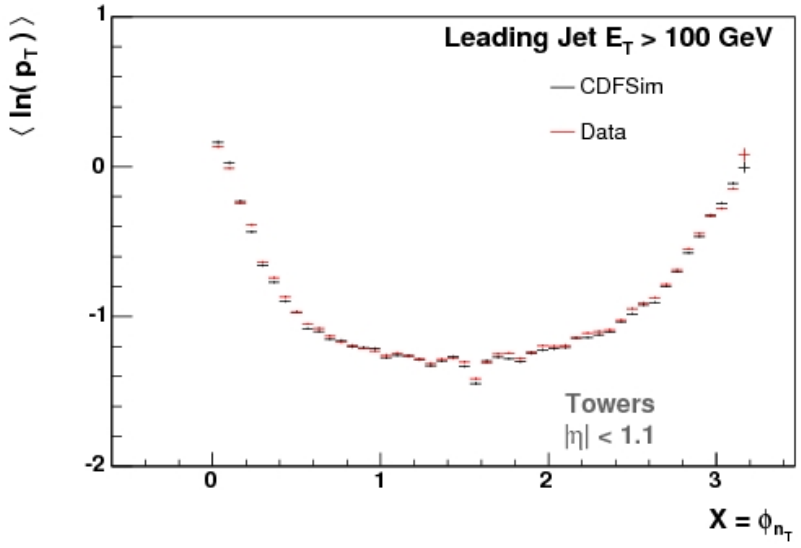

Figure 6: Mean value of the ln E_T of calorimeter towers in the central region $|\eta| < 1.1$, as a function of the angle between the 2D tower $\vec{p_T}$ and the transverse thrust axis $\vec{n_T}$. The label CDFSim refers to Pythia Tune A MC after full detector simulation.

7.2 Tracks

While our ultimate measurements are based on calorimeter information in the pseudorapidity range $|\eta| < 3.5$, restricting ourselves to the central region $|\eta| < 1.1$ makes possible the use of precision tracking to supplement our understanding of the flow of energy in dijet events. The primary advantage to this being that tracks allow us to focus on particles originating from the primary vertex while rejecting those produced by other sources.

A full description of CDF track reconstruction can be found in [10] [11]. In order to select signal tracks we apply the standard COT quality cut requiring $\chi^2_{fit} < 6.0$. This cut removes poorly reconstructed and spurious tracks. Furthermore, we consider only tracks with $p_T > 0.3$ GeV; below this threshold charged particles are expected to loop inside the magnetic field.

Additionally, to remove tracks which do not originate from the primary interaction we apply a cut on the Δz of each track. This parameter is defined as the difference between the z position of the track at the point of closest approach to the beam-line and the z position of the primary vertex. We then require that $|\Delta z| < 5\sigma_{\Delta z}$, where the resolution,$\sigma_{\Delta z}$, is determined for different types of tracks based on the number of SVX and COT hits. The values of $\sigma_{\Delta z}$ are summarized in Table 2.

Tracks coming from γ-conversions and K^0 and Λ decays are removed using a combination of cuts on impact parameter and the distance R_{conv}. The impact parameter is defined as the shortest distance in the r-ϕ plane between the interaction point and the trajectory of the particle. It can be shown that for electrons and positrons originating

Table 2: The resolution of track Δz and impact d_0 parameters evaluated for different categories of tracks based on the number of SVX and COT hits.

Algorithm	$\sigma_{\Delta z}$, cm	σ_{d_0}, mm
COT-only	1.20	0.110
Inside-Out (IO)	0.60	0.013
Outside-In $r\phi$	1.80	0.020
Kalman Outside-In $r\phi$	1.80	0.020
Outside-In stereo	0.40	0.014
Kalman Outside-In stereo	0.40	0.014
Outside-In 3D	0.21	0.0095
Kalman Outside-In 3D	0.21	0.0095
SVX Only	0.78	0.020

from γ-conversions

$$R_{conv} = \sqrt{\frac{d_0 p_T}{0.15B}}, \tag{11}$$

where p_T is the transverse momentum of the charged particle in GeV/c, B is the magnetic field in Tesla and R_{conv} is measured in meters. Monte Carlo studies have shown that placing the requirements $|d_0| < 5 \cdot \sigma_{d_0}$ *or* $R_{conv} < 13$ cm on tracks is more efficient in removing this background than either of these cuts alone. Incidentally, the value $R_{conv} = 13$ cm is motivated by the location of SVX port cards where a majority of these secondary interactions occur in the MC simulations and data. The resolution of the impact parameter, σ_{d_0}, varies for different types of tracks based on the number of SVX and COT hits. The measured values of σ_{d_0} are summarized in Table 2.

It is worth noting that the track cuts outlined above are identical to those used in past CDF analyses in Run II, namely CDF Note 7847 and CDF Note 8357. Nevertheless, to verify the effectiveness of track quality cuts we compare the momentum distribution of tracks (see Fig. 8) as well as the azimuthal distribution of tracks with respect to the thrust axis (see Fig. 7). Note that in these plots the label "CDFSim tracks" refers to reconstructed tracks after MC hadrons have been propogated through the detector using full CDF simulation which includes the simulation of conversions and in-flight decay. The agreement in these distributions confirms that our cuts remove most of the backgrounds.

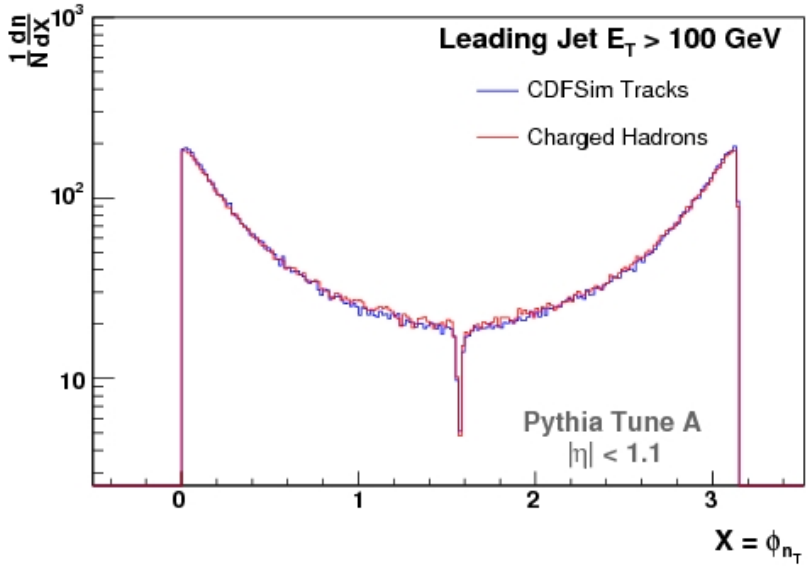

Figure 7: Distribution in ϕ of PYTHIA Tune A charged hadrons relative to the transverse thrust axis, compared to Monte Carlo tracks after full detector simulation for the entire central region $|\eta| < 1.1$

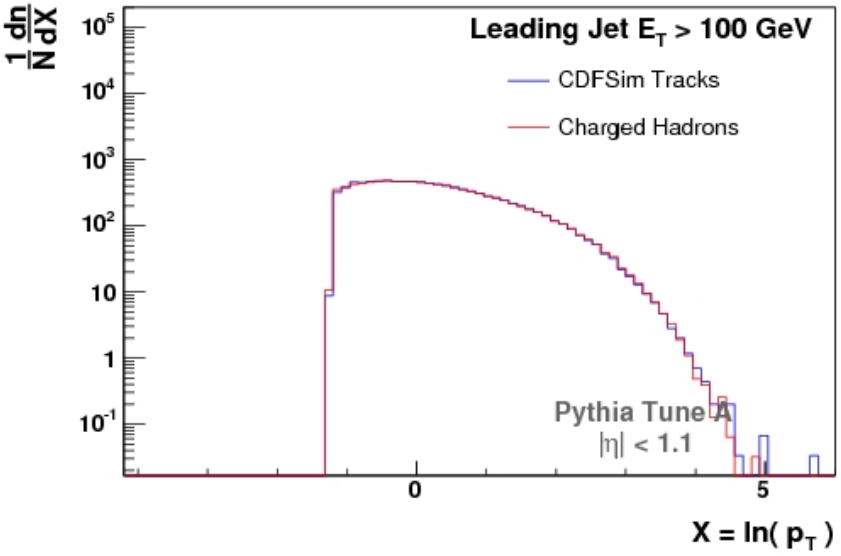

Figure 8: Inclusive momentum distributions of PYTHIA Tune A charged hadrons and PYTHIA Tune A tracks after full detector simulation for the entire central region $|\eta| < 1.1$

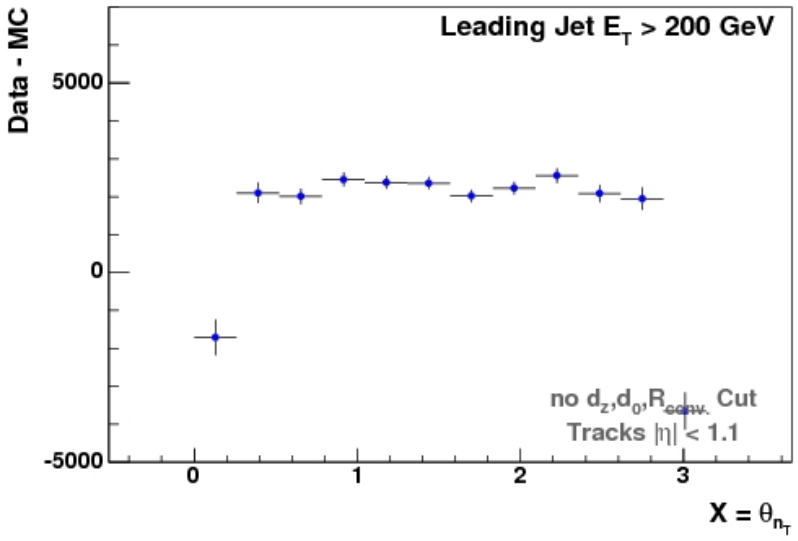

Figure 9: Difference between Data and Monte Carlo in the distribution of tracks as a function of the angle between the 2D track p_T and the transverse thrust axis n_T over the entire central region $|\eta| < 1.1$

Curiously, if we relax the cuts on d_z, d_0, and R_{conv} and compare Data and Pythia Tune A, we observe that there are many more rejected tracks in the Data than there are in the simulation (see Fig. 10). Furthermore, this excess is distributed uniformly (Fig.9), but is clearly most prominent in the region away from the primary energy flow ($\phi_{n_T} \sim \pi/2$) where the relative overage is $\sim 30\%$ (tracks are measured with $p_T > 300$ MeV). The same plot for calorimeter towers (Fig.11) reveals a similar excess of $\sim 40\%$ in the region away from the transverse thrust axis (towers are measured with $E_T > 100$ MeV). Additional studies suggest that this excess is the result of an underestimation in the amount of detector material in the CDF simulation package.

At the level of the calorimeter, these additional particles from secondary interactions appear as if they are simply part of the underlying event. In effect, they can make events look broader than they actually are. However, we anticipate this additional contribution to cancel-out in the final observable constructed (*i.e.*, in the weighted difference of the mean values of the transverse thrust and thrust minor).

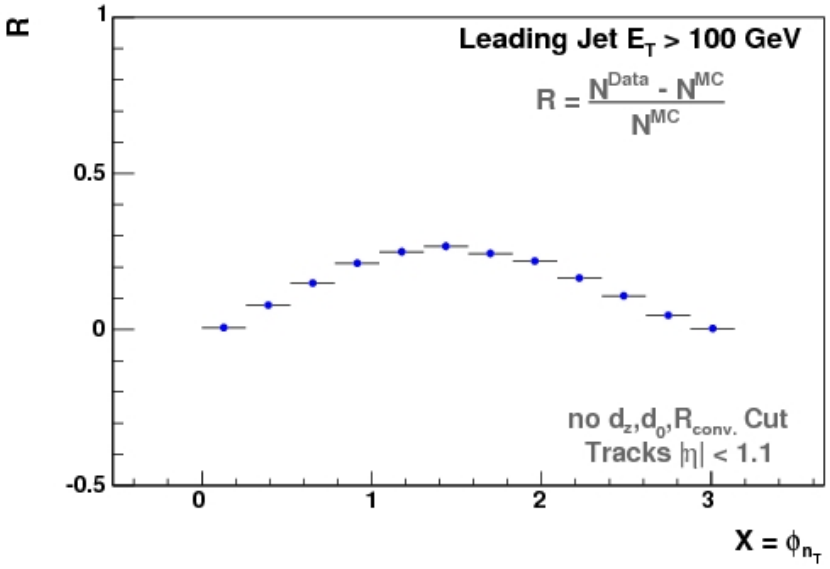

Figure 10: Relative difference between Data and Monte Carlo in the distribution of tracks as a function of the angle between the 2D track p_T and the transverse thrust axis n_T over the entire central region $|\eta| < 1.1$

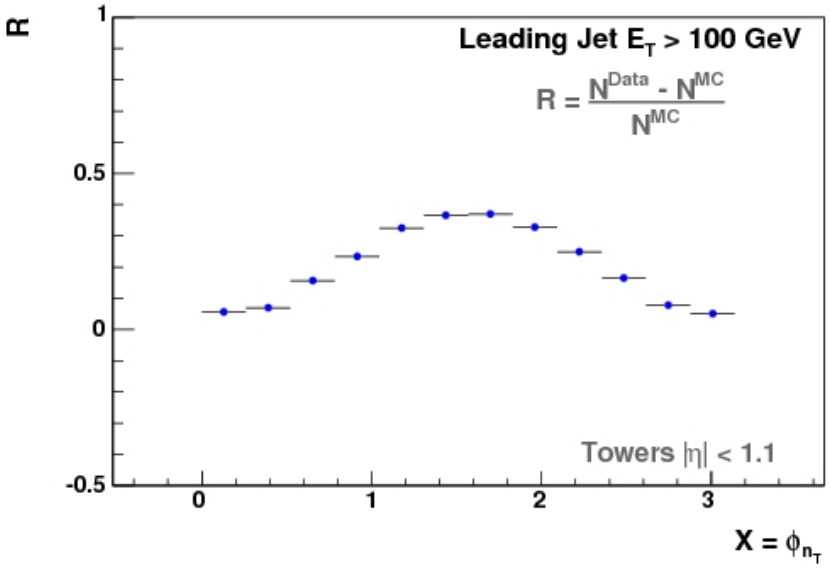

Figure 11: Relative difference between Data and Monte Carlo in the distribution of towers as a function of the angle between the 2D tower p_T and the transverse thrust axis n_T over the central region $|\eta| < 1.1$

8 Detector Effects

In general, the measurement of the event shapes may be distorted by the finite position and energy resolution of the detector. In this section we attempt to understand, at least qualitatively, how our detector instrumentation affects the observables measured. Figures **??** shows the mean values of the transverse thrust and thrust minor as a function of the leading jet energy for Pythia Tune A at the hadron level and at the calorimeter level after full CDF detector simulation. The plot indicates a relatively small effect of the detector instrumentation on the observables. The corresponding plot of the weighted difference between these two variables, Figs.14, reveals that on the scale of this final observable a noticeable systematic effect is present due to the simulation. Possible sources for this shift have been identified and investigated as follows:

- Charged particles traveling through a magnetic field experience the Lorentz force law which ultimately bends the trajectory of the particle from its straight line path. As a result, the energy flow of an event at the level of the calorimeter may appear broader than in the absence of a magnetic field. To estimate the magnitude of this effect on the final observable, MC particles at the hadron level were propogated to the first active layer of the calorimeter under the influence of a 1.41 Tesla B-field. The direction of the particle at this point is taken to be the location of the particle relative to the z position of the primary interaction point.

- The processes leading to electromagnetic and hadronic showers in a calorimeter are largely statistical in nature and therefore the energy resolution of the detector is subject to statistical fluctuations. To estimate the effect of the resolution, if any, on our final observable we smear (according to a gaussian distribution) the energy of the final MC particles by 1σ. For photons and electrons $\sigma_{EM}/E_T = 13.5\%/\sqrt{E_T}$ while for all other particles $\sigma_{HAD}/E_T = 75\%/\sqrt{E_T}$

- In the central region each calorimeter tower is $\Delta\eta \times \Delta\phi = 0.1 \times 15^\circ$ in size while in the plug region the calorimeter towers are $0.2 - 0.6 \times 15^\circ$ in spatial dimensions. When a particle above threshold is detected, the location returned by the system is the center of the tower and not the exact location of the shower within the tower. As a result, there is a mismeasurement associated with the granularity of the calorimeter. In an effort to understand this effect on our final observable, the segmentation of the calorimeter is imposed on MC particles at the hadron level.

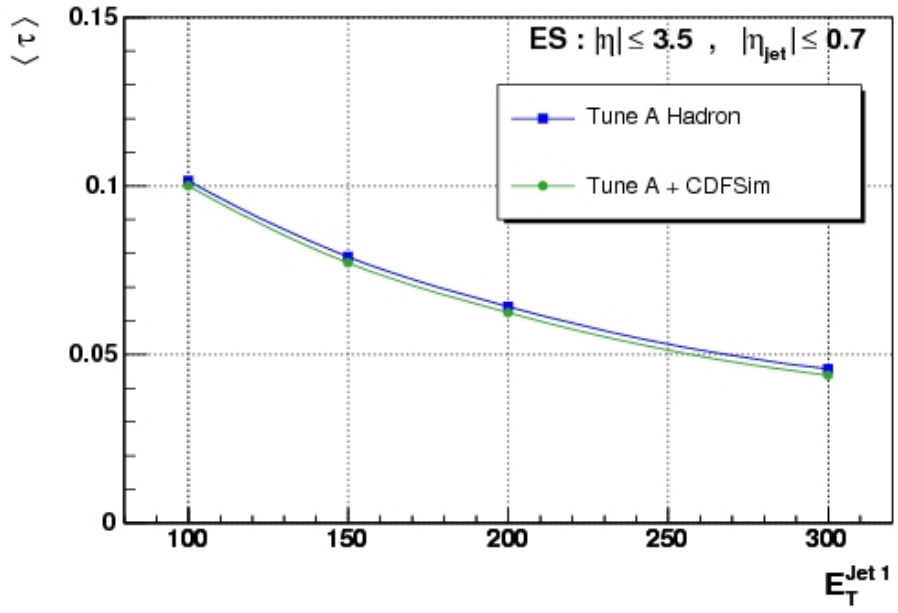

Figure 12: The effect of CDF detector simulation on the mean value of the transverse thrust as a function of the leading jet enery.

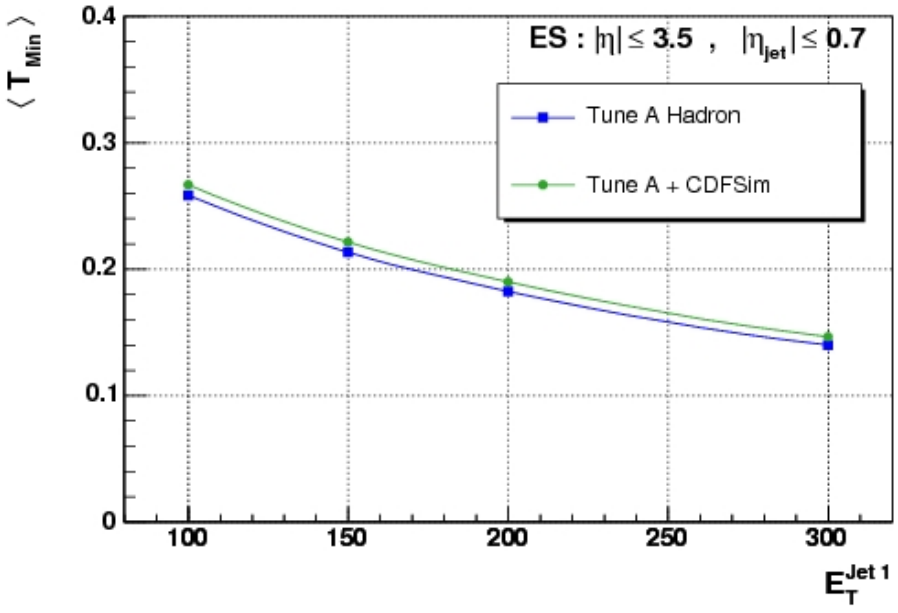

Figure 13: The effect of CDF detector simulation on the mean value of the transverse thrust minor as a function of the leading jet energy.

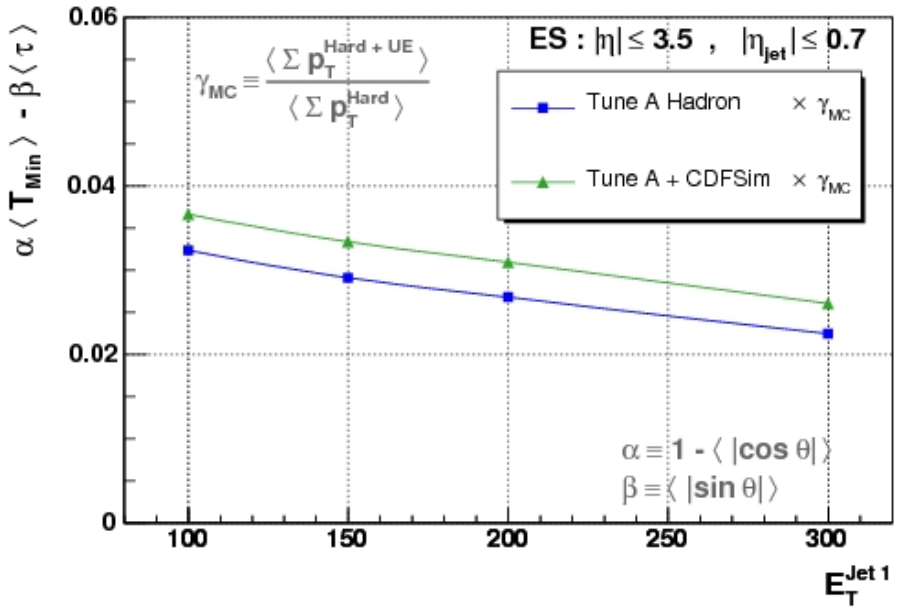

Figure 14: The effect of CDF detector simulation on the final observable constructed, the weighted difference in the mean values of the transverse thrust and thrust minor.

The results of these "itemized" detector effects are shown for the event shapes in Figure 16 and for the final observable in Figure 17. The granularity of the calorimeter appears as the primary source of the instrumental effect observed in the full detector simulation. Other detector effects include the sharing of energy between towers and the energy response of the calorimeter. However, all of these effects are incorporated into the full GEANT detector simulation. Ultimately, the difference in the final observable between the MC at the hadron level and detector level shall be quoted as a correction factor to the data.

Finally, the event shapes are defined theoretically over all particles in the final state, including those with arbitrarily small momenta. In an effort to understand how a cut on the transverse energy affects the observables, we vary the E_T threshold on towers from 100 MeV (default) through 200 and 300 MeV. Figures 18,19 shows the result of this variation on the mean values of the thrust and thrust minor. Clearly the events appear narrower as we cut-out more towers. However, Figure 20 shows that for the leading jet energies studied in this note, the final observable is rather insensitive to the cut on transverse momentum.

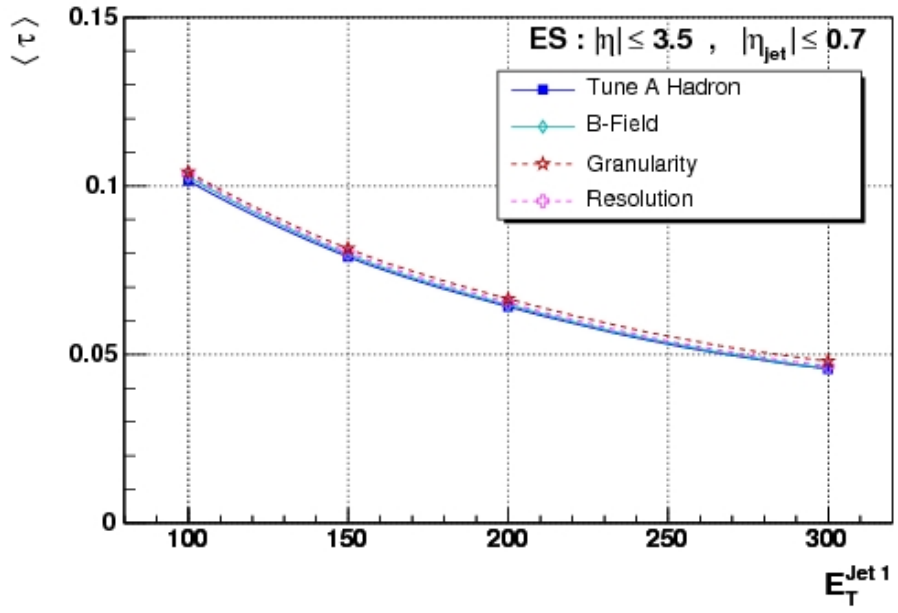

Figure 15: Contribution of isolated instrumental effects on the transverse thrust.

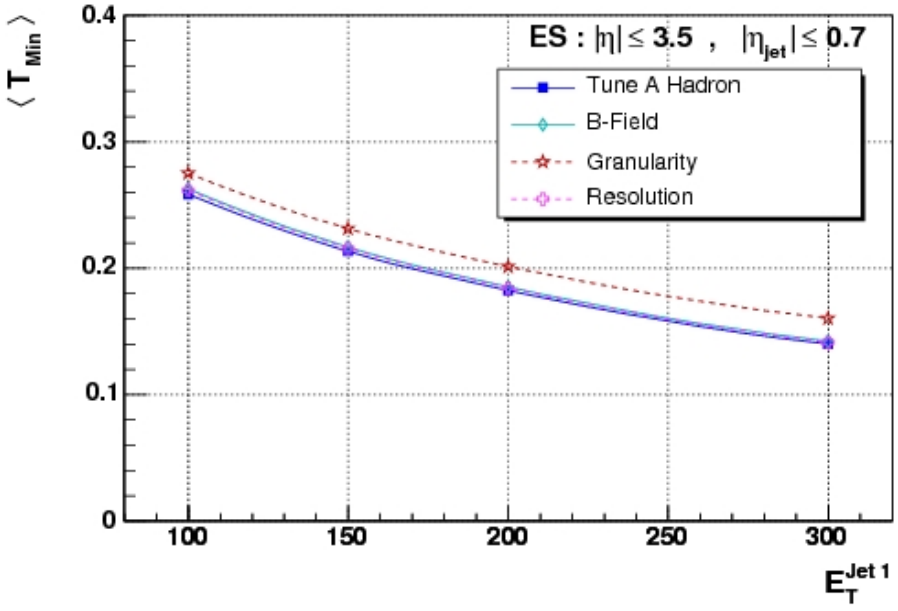

Figure 16: Contribution of isolated instrumental effects on the transverse thrust minor.

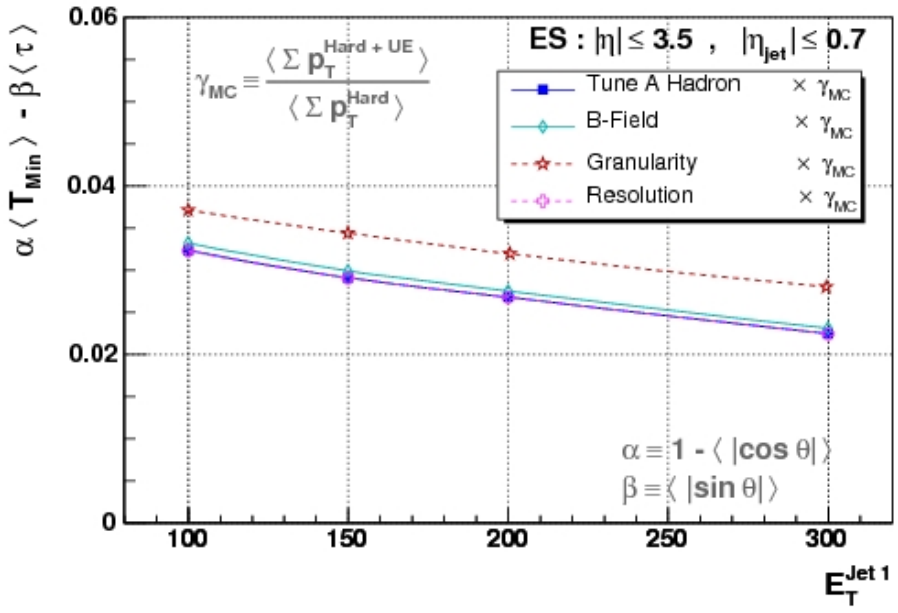

Figure 17: Contribution of isolated instrumental effects on the weighted difference of the mean values of the transverse thrust and thrust minor.

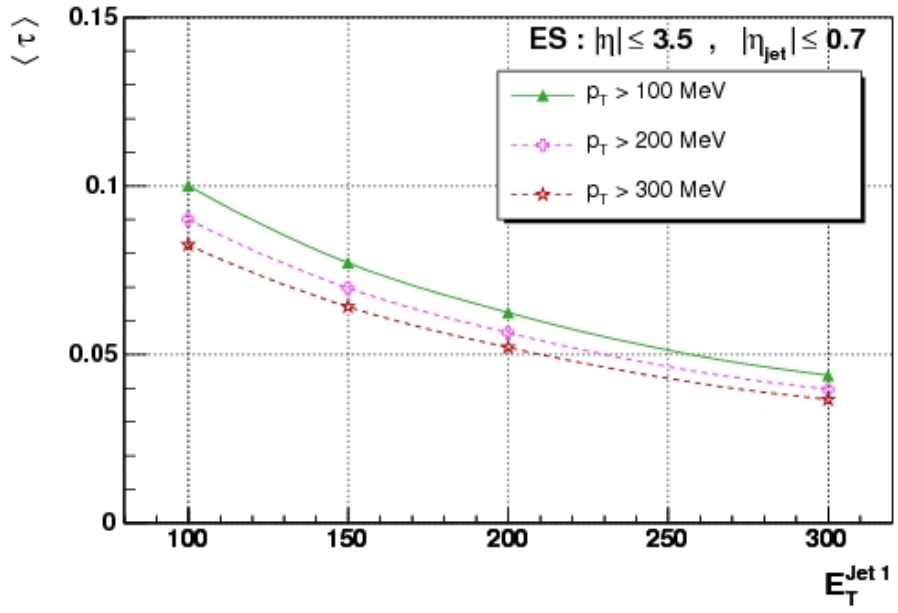

Figure 18: Effect of tower E_T threshold on the mean value of the the transverse thrust as a function fo the leading jet energy.

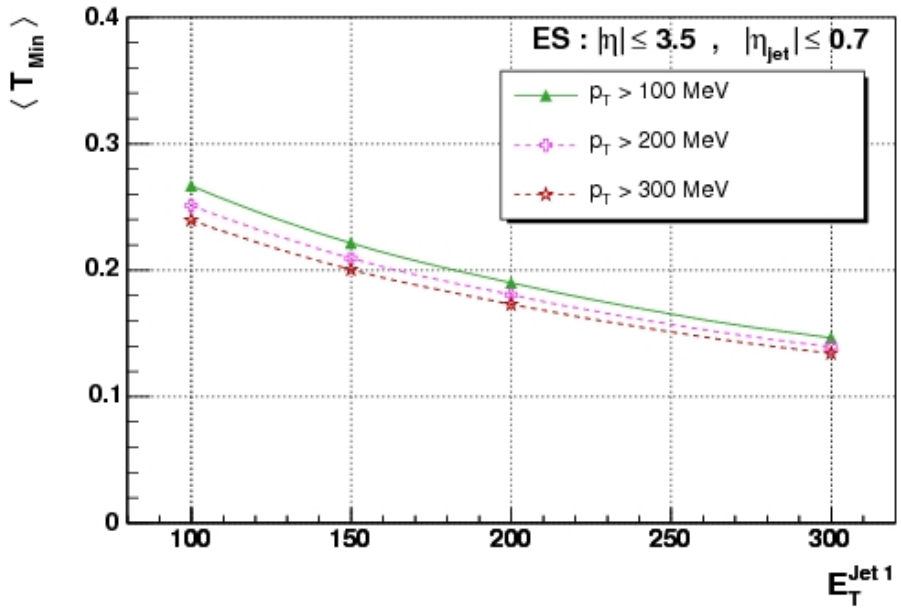

Figure 19: Effect of tower E_T threshold on the mean value of the the transverse thrust minor as a function fo the leading jet energy.

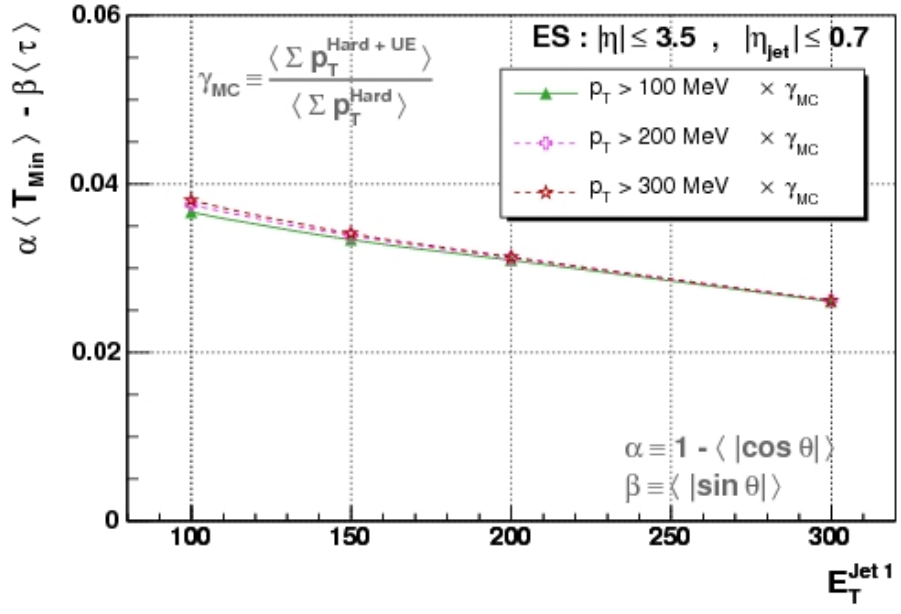

Figure 20: Effect of the tower E_T threshold on the weighted difference in the mean values of the transverse thrust and thrust minor.

9 Systematic Uncertainty

The sensitivity of our final observable to various uncertainties in the event selection procedure is evaluated as follows. For each source of systematic uncertainy, a "default" and "deviated" observable is constructed. The "default" observable is the result of the standard set of cuts defined earlier in this chapter, while the "deviated" observable is the result of varying a particular parameter by some amount within it's uncertainty. For each leading jet energy sample a scale factor is produced by taking the ratio of the "deviated" and "default" values of the final observable:

$$\epsilon = \frac{C(\langle\tau\rangle, \langle T_{Min}\rangle)_{deviated}}{C(\langle\tau\rangle, \langle T_{Min}\rangle)_{default}} \tag{12}$$

The difference between $C(\langle\tau\rangle, \langle T_{Min}\rangle)$ in the Data with and without this scale factor is then taken as a measure of the systematic uncertainty. Each individual source of uncertainty is then added in quadrature to the statistical uncertainty in each data point.

9.1 Jet Energy Scale

To evaluate the uncertainty due to the jet energy corrections, we use a parametrization that under- and over-estimates the jet energy by one standard deviation in the jet energy scale and then re-run our event selection. The difference between the default and the deviated observable is assigned a systematic uncertainty.

9.2 Containment in the Detector

The primary interaction vertex is required to lie within 60 cm from the center of the detector in order to ensure that the majority of the event is contained within the detector. The analysis of event shapes uses calorimeter information in the far forward regions of the detector. As a result, the further a collision occurs from the nominal interaction point the greater the possiblity that particles fall beyond the detector's converage. To evaluate the uncertainty due to this effect we require a tighter cut on the z position of the primary vertex. The difference in the observable between the default and the tight cut is then assigned as a systematic uncertainty.

9.3 Accelerator Induced Backgrounds

In the event selection we specifically require events with a single vertex; however, it is possible that two vertices that lie very close to each other can be reconstructed as a single vertex. This "pile-up" effect is especially likely at high values of the instantaneous luminosity. To evaluate the uncertainty due to this effect we separate events in each data sample into high and low luminosity subsets with approximately equal number

of events. The final observable is then compared between subsets and the difference is taken as a measure of the systematic uncertainty.

10 Results

10.1 NLO+CAESAR vs. PYTHIA

Figure 21 shows a comparison of the distributions of Transverse Thrust and Thrust Minor between dedicated theoretical prediction, labeled "CAESAR+NLO", and PYTHIA at the parton level and after hadronization. These plots reveal that apart from a shift away from the 2-jet limit over nearly the entire range of the variables, the Monte Carlo actually reproduces the shape of the distributions reasonably well. The shift can be seen more concisely in Figure 22 which shows the mean values of the observables as a function of the leading jet E_T. We note that the discrepancy between theorists' predications and PYTHIA at the parton level decreases with increasing jet energy. This difference is likely due to the beam remnants and the amount of ISR present in the MC which is set to the Tune A setting (Parp[67] = 4), but may also be the result of the relatively large parton shower cutoff (Q_o = 1 GeV) in the MC[4]. Furthermore, we note that the hadronization model in PYTHIA has the effect of shifting the distributions towards larger event shape values–a result expected from LEP studies [5]. However, we see that these discrepancies vanish from the final observable constructed, $C(\langle\tau\rangle, \langle T_{Min}\rangle)$, (see Fig. 23).

10.2 NLO+CAESAR vs. Tune A

Figure 24 shows a comparison of the event shape distributions between theorists' predictions, PYTHIA without MPI, and Tune A. Clearly, the underlying event not only shifts the means towards higher values, but also significantly distorts the over-all shape of the distributions. Turning to the plots of the mean values as a function of leading jet energy, Figures25 we observe in comparing Tune A at the parton and hadron levels, that the underlying event appears to dampen the effects of hadronization on the distributions. In some sense, the additional particles from the underlying event saturate the event shapes distributions to a point where the "re-shuffling" of momenta that occurs at hadronization has little effect on the observable. Finally, we note that in the final observable constructed, $C(\langle\tau\rangle, \langle T_{Min}\rangle)$, the contribution from the underlying event cancels (as expected) and good agreement is seen between theorists' predictions and Pythia Tune A.

[4]While a lower parton shower cutoff would produce more final state particles, at least some of those particles would be more colinear with the initial outgoing parton, and therefore may lead to smaller event shape values.

10.3 Data

In this section we present the experimental results of the measurement of event shapes in $p\bar{p}$ collisions at $\sqrt{s} = 1.96$ TeV. The results are compared to resummed theoretical predictions that have been matched to fixed order results both of which are at "next-to-leading" accuracy. Comparison to PYTHIA Tune A are also presented.

The distributions of the transverse thrust and thrust minor, uncorrected for detector effects, are presented in Figure 27 for the leading jet energies 100, 150, 200, and 300 GeV. The distributions in data are shifted by roughly a constant amount relative to the distributions in PYTHIA Tune A after detector simulation; however, the over-all shape is well reproduced by the MC. Both Data and PYTHIA Tune A show significant departures in shape relative to the distributions provided by theorists, which do not incorporate an underlying event.

The evolution of the mean values of these two observables is presented in Figures28. Here, again, the data have not been unfolded to the particle level. These plots highlight the relatively small detector effects in the measurement of the transverse thrust and thrust minor as well as the comparatively larger, but roughly constant offset between data and simulation.

Finally, Figures 29 shows the weighted difference between the mean values of the transverse thrust and thrust minor as a function of the leading jet E_T. This observable ultimately allows for a direct comparison between data and the dedicated predictions of theorists (labeled 'CAESAR + NLO') which do not incorporate an underlying event. In this plot detector effects have been accounted for; to reflect this, the data is labeled "Unfolded". The figure shows good general agreement between theorists predictions, Pythia Tune A, and data. The unfolded data and it's associated undertainties are listed in Table 3.

References

[1] S. Bethke, Nucl. Phys. Proc. Suppl. **135**, 345 (2004), hep-ex/0407021.

[2] M. Dasgupta and G. P. Salam, J. Phys. **G30**, R143 (2004), hep-ph/0312283.

[3] DELPHI, P. Abreu *et al.*, Z. Phys. **C73**, 11 (1996).

[4] T. Kluge, (2006), hep-ex/0606053.

[5] P. A. Movilla Fernandez, S. Bethke, O. Biebel, and S. Kluth, Eur. Phys. J. **C22**, 1 (2001), hep-ex/0105059.

[6] A. Banfi, G. P. Salam, and G. Zanderighi, JHEP **08**, 062 (2004), hep-ph/0407287.

[7] A. Banfi, G. Marchesini, G. Smye, and G. Zanderighi, JHEP **08**, 047 (2001), hep-ph/0106278.

[8] Z. Nagy, Phys. Rev. **D68**, 094002 (2003), hep-ph/0307268.

[9] A. Banfi, G. P. Salam, and G. Zanderighi, JHEP **03**, 073 (2005), hep-ph/0407286.

[10] CDF Collaboration, R. Wagner and et. al., FERMILAB-PUB **96/390-E** (1996).

[11] C. Hays *et al.*, Nucl. Instrum. Meth. **A538**, 249 (2005).

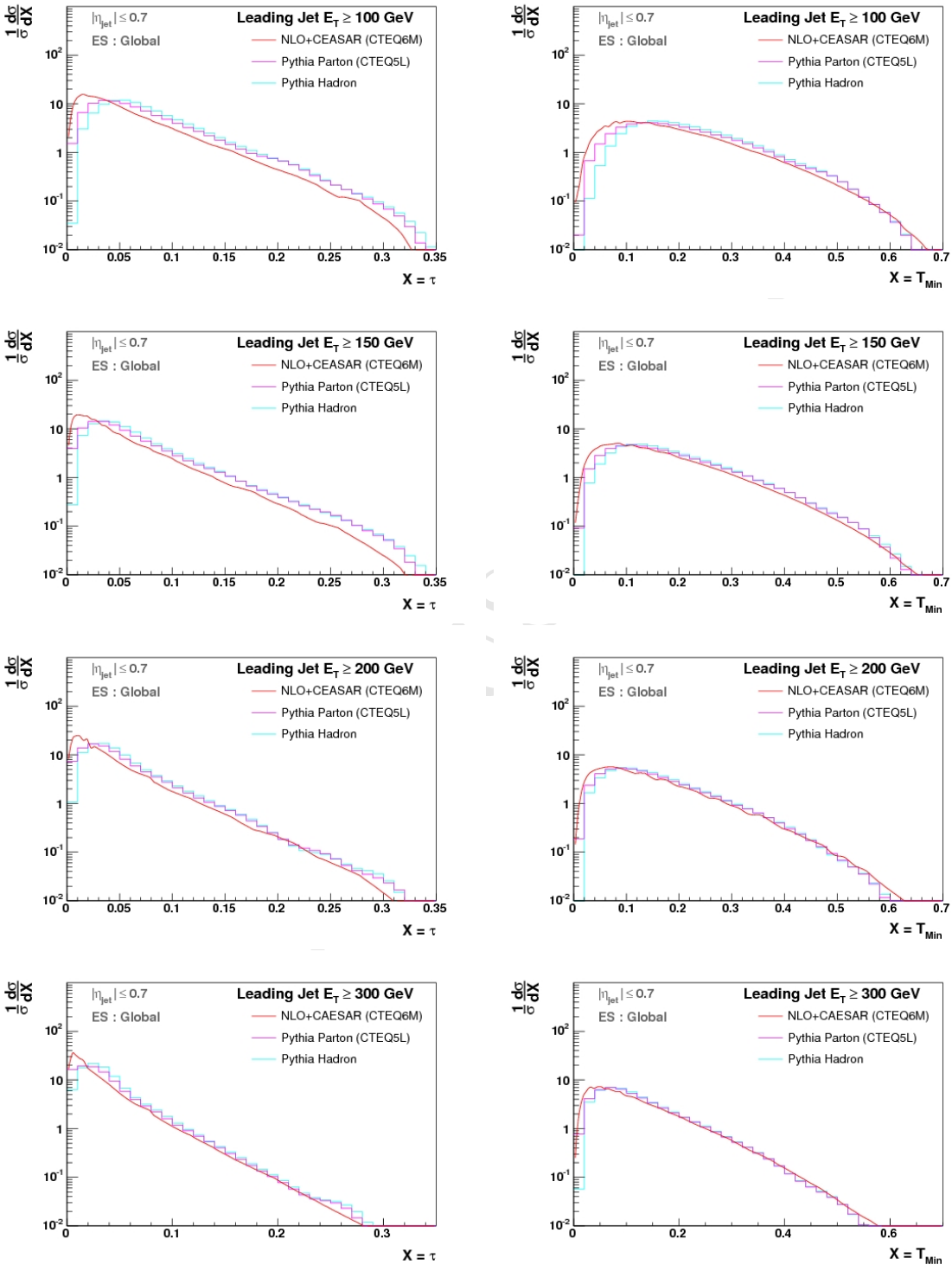

Figure 21: Distributions of the transverse thrust and thrust minor for leading jet energies 100, 150, 200, and 300 GeV. Comparison is made between theoretical predictions at (NLO+NLL) accuracy and PYTHIA without an UE.

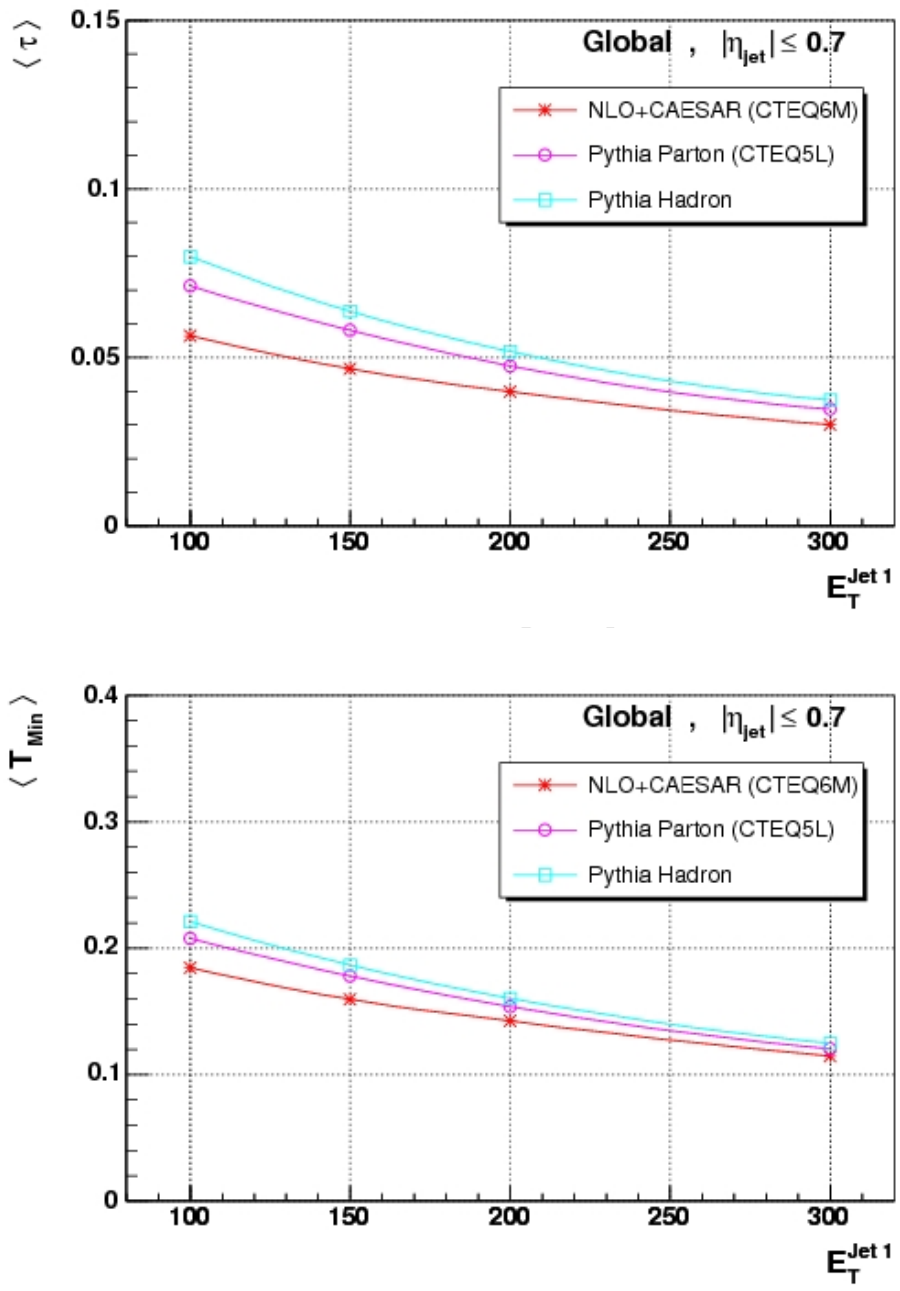

Figure 22: Evolution of the mean values of the transverse thrust and thrust minor as a function of the leading jet energy. Comparison is made between theoretical predictions at (NLO+NLL) accuracy and PYTHIA without an UE.

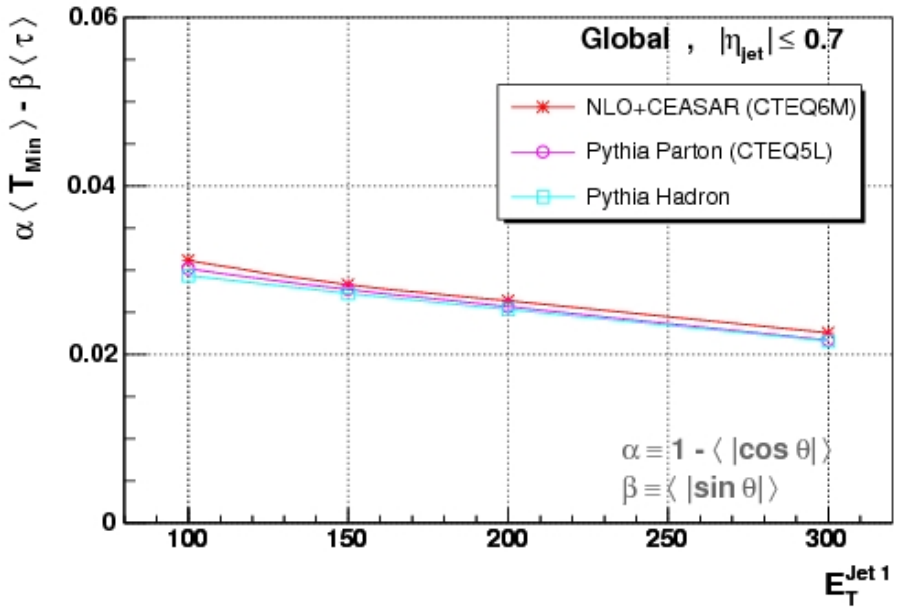

Figure 23: The weighted difference of the mean values of thrust and thrust minor as a function of the leading jet energy. Comparison is made between theoretical predictions at (NLO+NLL) accuracy and PYTHIA without an UE.

Table 3: Summary of data points and uncertainties in the final observable constructed

E_T^1 (GeV)	$C(\langle\tau\rangle, \langle T_{Min}\rangle)$	Stat.	JES	Z_{vtx}	Lum.
100	3.57116e-2	4.508e-4	3.06e-5	4.84e-5	2.84e-4
150	3.33773e-2	7.378e-4	1.25e-4	1.56e-4	4.53e-4
200	3.16408e-2	5.901e-4	3.38e-4	6.06e-5	2.83e-4
300	2.72398e-2	1.490e-3	4.73e-4	7.67e-4	7.09e-4

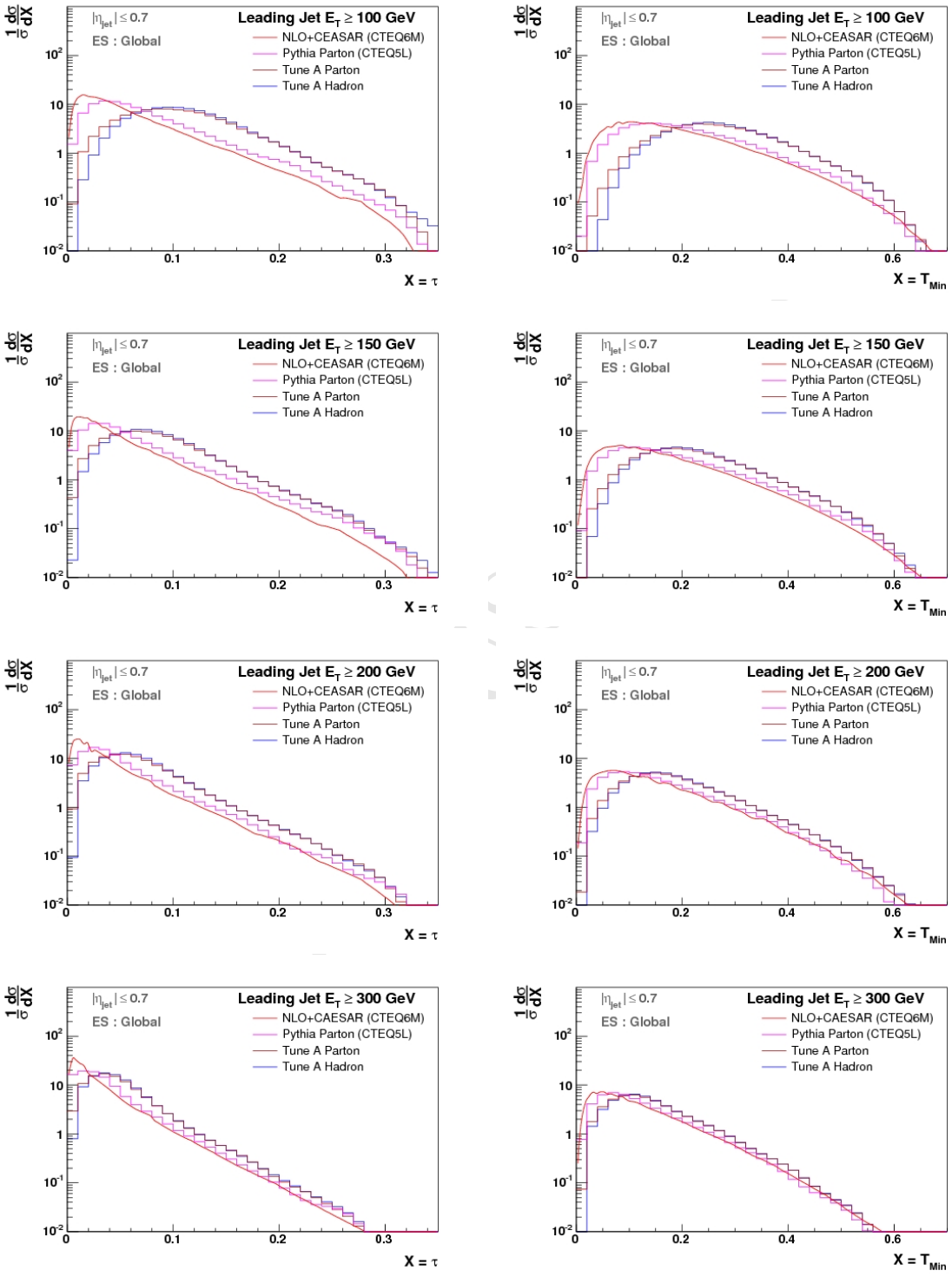

Figure 24: Distributions of the transverse thrust and thrust minor for leading jet energies 100, 150, 200, and 300 GeV. Comparison is made between theoretical predictions at (NLO+NLL) accuracy and PYTHIA with and without an UE.

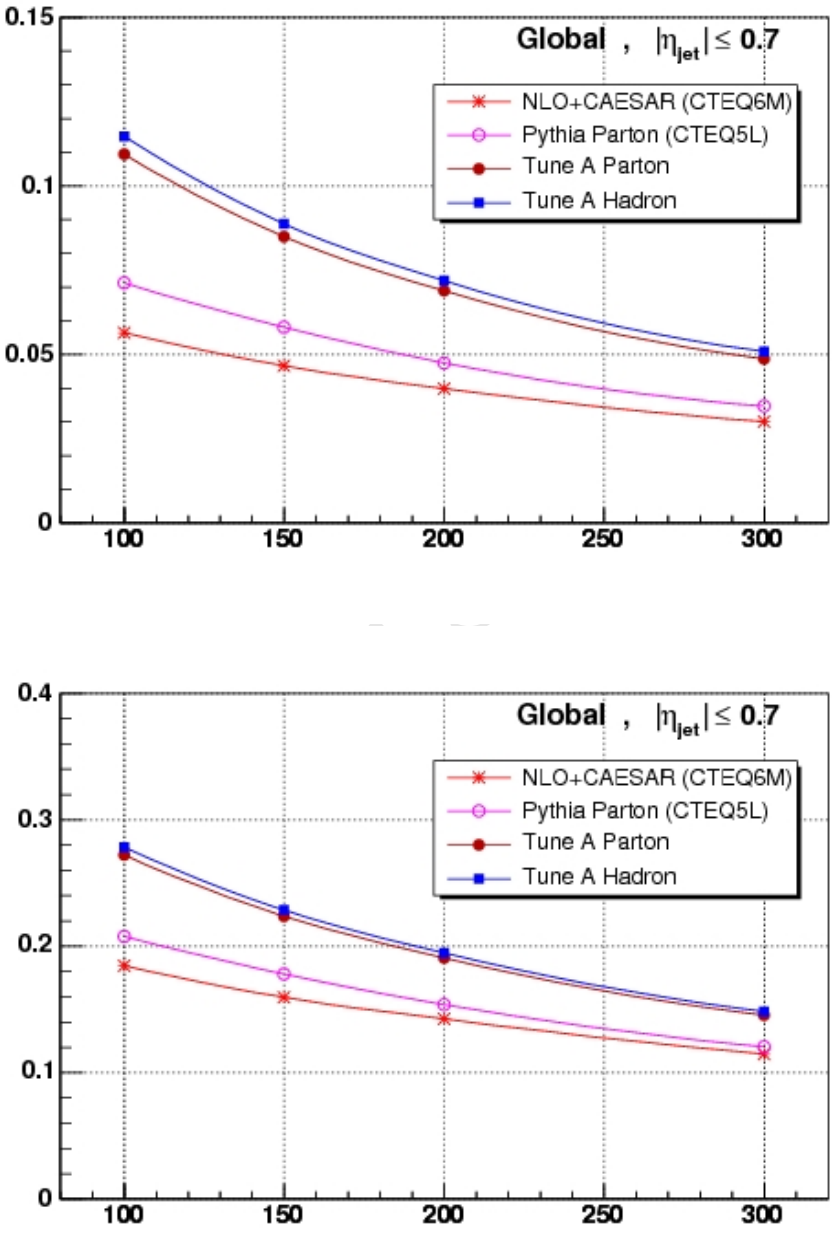

Figure 25: Evolution of the mean values of the transverse thrust and thrust minor as a function of the leading jet energy. Comparison is made between theoretical predictions at (NLO+NLL) accuracy and PYTHIA with and without an UE.

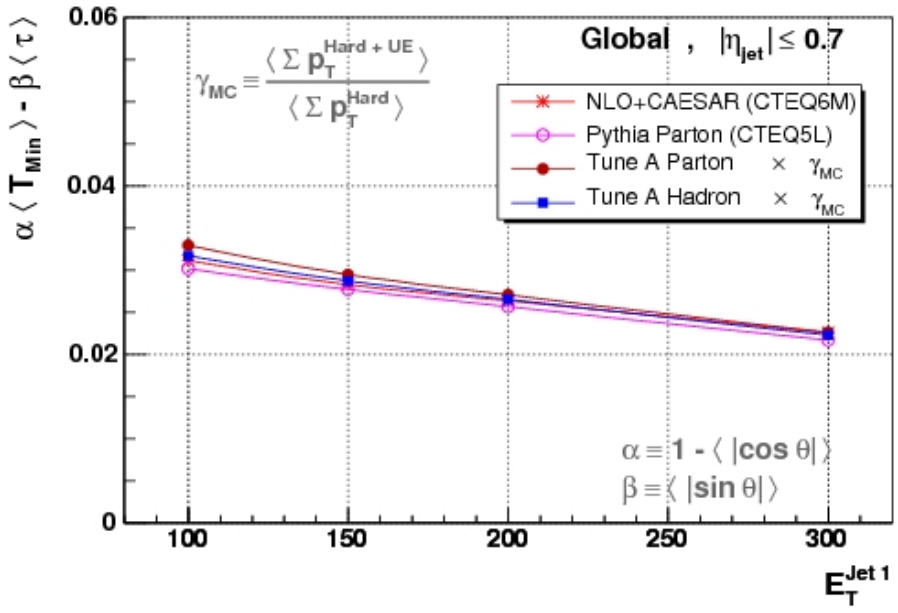

Figure 26: The weighted difference of the mean values of transverse thrust and thrust minor as a function of the leading jet energy. Comparison is made between theoretical predictions at (NLO+NLL) accuracy and PYTHIA with and without an UE.

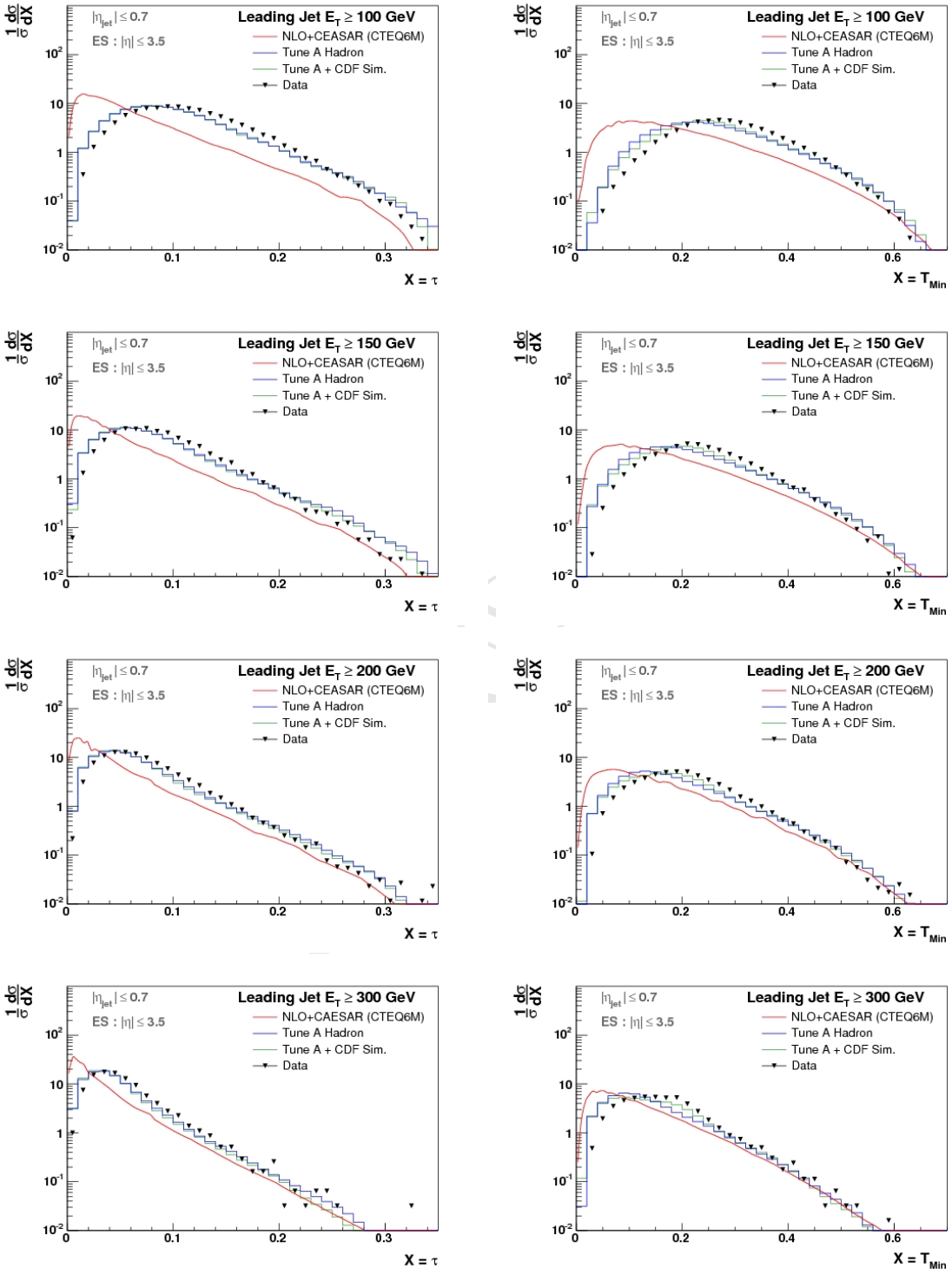

Figure 27: Distributions of the transverse thrust and thrust minor for leading jet energies 100, 150, 200, and 300 GeV. Comparison is made between theoretical predictions at (NLO+NLL) accuracy, PYTHIA Tune A at the hadron level as well as after detector simulation, and Data.

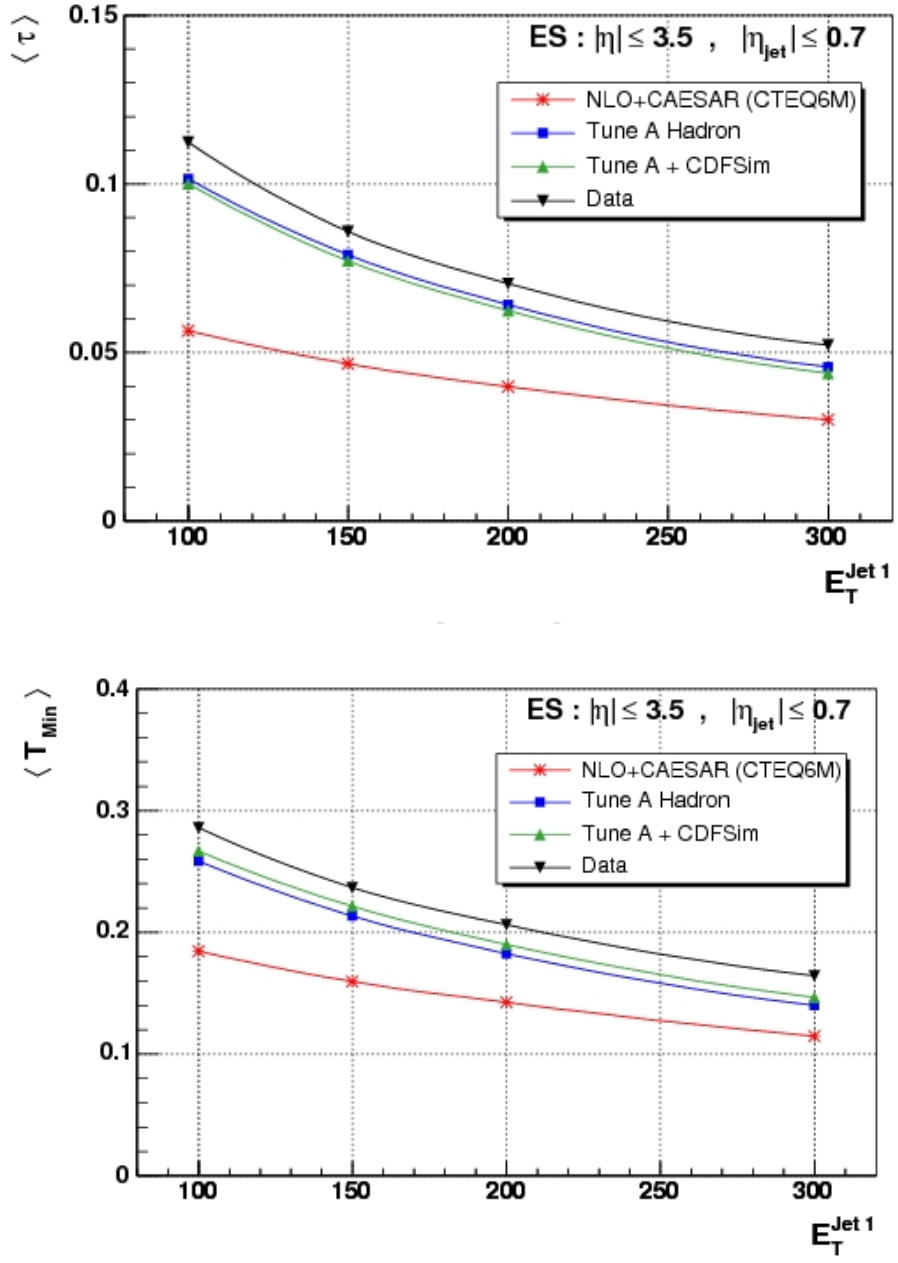

Figure 28: Evolution of the mean values of the transverse thrust and thrust minor as a function of the leading jet energy.Comparison is made between theoretical predictions at (NLO+NLL) accuracy, PYTHIA Tune A at the hadron level as well as after detector simulation, and Data.

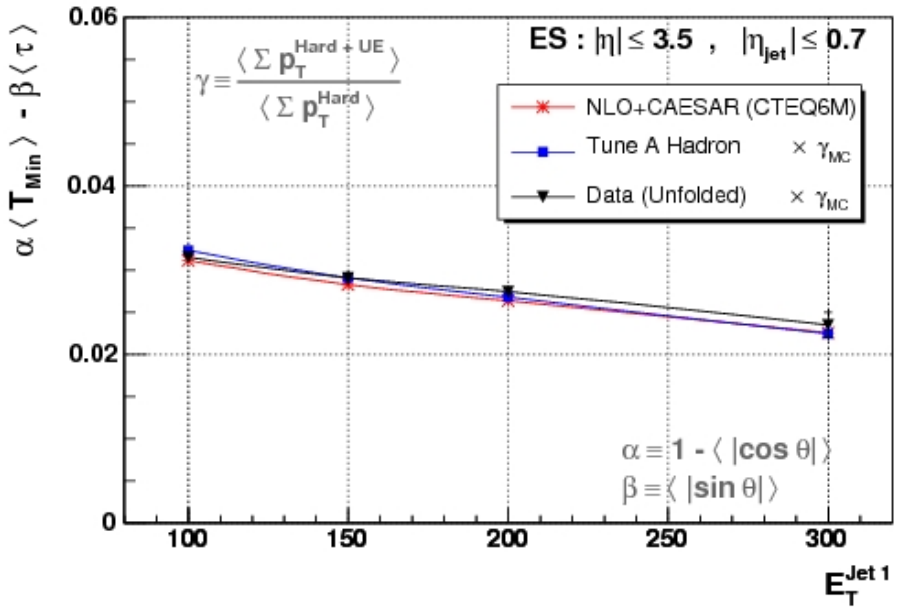

Figure 29: Plot of the weighted difference of the mean values of Thrust and Thrust Minor as a function of the leading jet energy for CAESAR+NLO, PYTHIA Tune A at the Hadron level and Data unfolded to the particle level. The smaller error bars correspond to statistical uncertainty only, while the larger bars correspond to statistical and systematic uncertainties added in quadrature.